ACTA METALLURGICA SLOVACA
2023, VOL. 29, NO. 2, 88-92

RESEARCH PAPER

METALLURGICAL INVESTIGATION OF DIRECT DRIVE FRICTION WELDED JOINT FOR AUSTENITIC STAINLESS STEEL

Ammar Jabbar Hassan[1], Billel Cheniti[2], Brahim Belkessa[2], Taoufik Boukharouba[1], Djamel Miroud[3], Nacer-Eddine Titouche[4]*

[1] Advanced Mechanics Laboratory (LMA), USTHB, BP. 32, El Alia 16111, Bab Ezzouar, Algiers, Algeria
[2] Research Center in Industrial Technologies, P.O. Box 64, Chéraga, 16014 Algiers, Algeria
[3] Science and Engineering Materials Laboratory (LSGM), USTHB, BP. 32, El Alia 16111, Bab Ezzouar, Algiers, Algeria
[4] Birine Nuclear Research Center, BP. 180, Ain Oussera, Djelfa, 17200, Algeria

*Corresponding author: e-mail: ajabbarhassan@usthb.dz, Advanced Mechanics Laboratory (LMA), USTHB, BP. 32, El Alia 16111, Bab Ezzouar, Algiers, Algeria

Received: 03.05.2023
Accepted: 25.05.2023

ABSTRACT

The present study investigates the metallurgical behavior of direct-drive friction-welded (DDFW) joints for high Cr-Ni-Mo steel (AISI 316). The selected welding conditions are rotation speed of 3000 rpm, friction time of 10 s, friction pressure of 130 MPa, forge time of 5 s, and forge pressure of 260 MPa. The results were conducted by macroscopic observation to detect flash and macro defects such as cracks or cavities, microscopic observation using to investigate the grain size before and after the welding process to detect the regions around the welding joint, microhardness observation along the axial direction to determine the dimension of welding regions, and X-ray diffraction (XRD) to show the thermal influence alone and evaluation of the thermo-mechanical properties of the as-welded case. The results for the macroscopic view showed that the narrow welding center did not exceed 600 µm and there were no macro cracks or defects, indicating a uniform structure. The microstructure exhibited a significant welded joint interface with microcavities and grain refinement of 10 µm, about three times smaller than the grain size of AISI 316, due to the creation of a highly plastically deformed zone (HPDZ), while the thermo-mechanically affected zone (TMAZ) formed in the neighboring area with a grain growth of about 100 µm, relatively enlarged three times compared to AISI 316 and ten times related to HPDZ. Thus, the high level of microhardness was investigated at the welding center and low values in the neighboring area were caused by the formation of the HPDZ and TMAZ, respectively. XRD also illustrated the concentration of gamma iron at the 111 level due to the grain refinement resulting from high plastic deformation.

Keywords: Austenitic stainless steel; AISI 316; Friction welding; highly plastically deformed zone; Thermo-mechanically affected zone

INTRODUCTION

Fusion welding methods are widely used to join Cr-Ni-Mo austenitic stainless steel [1], but problems such as oxidation, cracking, and the formation of brittle intermetallic compounds often result in poor welded joints. Solid-state welding processes, on the other hand, can produce joints at sub-fusion temperatures with minimum cracking and defects. Friction welding (FW) is one such method that can join similar and dissimilar materials with low cost, short processing times, low energy input, ease of setup, sub-melting temperatures, high reproducibility, and high joint efficiency [2, 3].

In the literature, the two most well-known functional methods of FW are friction stir welding (FSW) and DDFW [4]. FSW is a reliable welding technique for joining light metals, particularly aluminum and its alloys, for use in aerospace and automobile parts. It produces joints using a non-consumable tool to soften the metal by generating heat due to friction between the rotating tool and the workpieces. The material is then deformed plastically to create a significant welded joint [5, 6, 7].

On the other hand, DDFW is used to fabricate most mechanical parts, such as turbine shafts, truck axles, piston rods, electrical connections, and cutting tools [8]. This method is carried out by elevating the temperature between the two surfaces in contact under the effect of rotation speed and axial pressure. The first piece is connected to the stationary part, and the second piece is chucked to the rotating part. The latter supplies the welding energy between the two effective pieces to complete the welded joint [9].

Several studies have considered friction welding of austenitic stainless steel. Wang et al. [10] welded annealed AISI 304 using DDFW with 25 mm diameter rods. FW joints were made with a rotation speed of 1500 rev/min, friction pressure of 80 MPa, and forge pressure of 80 MPa for a forge time of 6 s. They showed that dynamic recrystallization occurred on the entire interface, and the welding zone contained equiaxed grains.

Liu and Fujii [11] used friction welding to join Ti64 to AISI 316L for a length of 100 mm and a diameter of 10 mm. They employed low rotation speeds of 40-300 rpm and high friction pressures of 400-500 MPa. High rotation speed provided a low temperature rising rate, and high friction pressure was utilized to produce a proper welding temperature that would result in a thin and strong intermetallic compound layer to avoid cracking

at the interface. High-quality FW of Ti64/SUS316L was produced productively using high rotation speed and suitable high friction pressure.

Titouche et al. [12] have studied the effect of DDFW on the characteristics of Ti-stabilized austenitic stainless steel (AISI 321) for thick tubes. The samples, 48 mm in length, were cut into thick-walled tubes with 8 mm inner and 14 mm outer diameter. They found that a few hundred microns of grain refinement structure were produced by dynamic recrystallization at the interface. The temperature reached the interface, and the stress concentration obtained the recrystallization conditions. While the thermo-mechanically affected zone in the neighboring consists of the partially deformed zone with larger and elongated grains. Corrosion resistance also improved at the interface related to the other regions due to grain refinement amplifying corrosion resistance. Cheniti et al. [13] have used DDFW for WC-Co to AISI 304L. They demonstrated a high level of hardness revealed in nano-scratch tests at the interface compared to AISI 304L.

During DDFW, there are two phases that can control that process: the friction and forge phases. Three conditions during the friction phase are rotation speed, friction time, and friction pressure, while two conditions during the forge phase are forged time and forge pressure [3, 4, 12, 13]. According to previous works, rotation speed and friction time [14], as well as friction pressure [15], are the most important conditions that affect the quality of the welded joint. Rotation speed has a main effect on the microstructure because it controls the cooling rate as well as the final deformation [16], and a reduction in rotation speed decreases the temperature-increasing rate [17].

In general, high friction pressure induces dynamic recrystallization at the interface, which causes grain refinement and increases the values of hardness [18]. Low friction pressure, on the other hand, results in a lack of bonding [15]. Increasing friction time leads to an increase in temperature, which supports plastic deformation and results in a larger thermo-mechanically affected zone (TMAZ). Thus, a longer friction time creates a higher working temperature that leads to material deformation [13]. To obtain high joint efficiency, forge pressure higher than that of friction pressure should be applied. However, an increase in forge pressure preserves the joint efficiency [19], as observed in the study of Hazra et al. [20]. Forge pressure creates dynamic recrystallization at the interface and leads to grain refinement, which is responsible for heat-affected zone (HAZ) formation [3].

This present study attempts to understand the microstructure behavior of DDFW for AISI 316 rods. The selected welding conditions were a rotation speed of 3000 rpm, a friction time of 10 s, a friction pressure of 130 MPa, a forge time of 5 s, and a forge pressure of 260 MPa. The results were investigated by macro-microscopic, microhardness, and XRD techniques. The study shows that the macro-microstructure investigation of the welded joint interface and neighboring region allows for the estimation and evaluation of the joint efficiency of AISI 316 during DDFW.

MATERIAL AND METHODS

Austenitic stainless steel is widely used in engineering fields, such as corrosive media, alimentation, and medical, and chemical applications. It is highly composed of Cr, Ni and Mo, as shown in **Table 1**, and is identified by the American Institute for Steel and Iron as AISI 316 with Ref. No. 4401. It has the same alloying elements as AISI 304, with the addition of Molybdenum (Mo 2.93%) to enhance corrosion resistance and properties at elevated temperatures. The metal used in this study was received in the laboratory as long shafts of 6 m length, which were cut into small pieces of 12 mm diameter and 45 mm length. The metallurgical study was conducted at LSGM, USTHB, Algeria. **Figs. 1a & b** show the microstructure of AISI 316 observed by optical microscopy and scanning electron microscopy (SEM), respectively, revealing equiaxed austenite grains ranging from 25-50 μm.

Table 1 Alloying elements of AISI 316 (wt.%)

C	Mn	Si	P	S	Mo	Cr	Ni
0.070	1.500	0.670	0.030	0.021	2.93	17.93	9.95

In this study, a welding machine was used to join the pieces, which was designed and fabricated as a DDFW machine, as mentioned in previous studies [3, 4, 15]. The maximum rotation speed for this machine is 3000 rpm, and the maximum pressure that can be applied is 300 MPa. The friction welding conditions were chosen based on previous studies and related to the test piece diameter and mechanical and metallurgical properties of the base metal. The selected welding conditions are a rotation speed of 3000 rpm, friction time of 10 s, friction pressure of 130 MPa, forge time of 5 s, and forge pressure of 260 MPa.

NIKON SMZ 745T was used for macroscopic observations to detect flash and macro defects such as cracks or cavities. On the other hand, microstructure observations were carried out using two methods to investigate the grain size before and after the welding process and to detect neighboring regions more accurately. The first method involved scanning electron microscopy (SEM) using JEOL JSM-6360 at magnifications of × 55, × 130, × 500, and × 1000. The second method used optical microscopy with a NIKON ECLIPSE LV100ND at magnifications of × 50, × 100, and × 200. The sample for these studies was cut using a Presi mecatome T180 cutting machine. The test piece was fixed in cold-curing epoxy resin, polished with wet SiC abrasive paper up to 1200 grit, and then polished with 1 μm diamond polishing paste. The sample was cleaned with deionized water and dried using hot air. The electrolytic etching was carried out using 10 g of oxalic acid hydrate and 90 ml of water at 15 V for 300 s via STRUERS LECTROPOL-5.

Vickers microhardness measurements were performed along the axial direction within 3 mm on the rotating side and 4.5 mm on the stationary side. The investigation of microhardness profiles along that direction permitted the differentiation of regions around the welded joint. The SHIMADZU HMV microhardness tester was used for measurements at room temperature conditions according to ASTM E384 qualifications. A 100 N indentation load and a 10 s dwell time were used for the measurements. The test pieces were cut using a Presi mecatome T180 cutting machine and polished up to 1200 grit with wet SiC abrasive paper, followed by 1 μm diamond paste on a cloth disc. The samples were then degreased with ethanol and cleaned with deionized water.

XRD was carried out using X'Pert PRO PAN analytical for the base metal, as-welded cases, and for heat-treated AISI 316 (temperature of 819°C, soaking time of 30 min, and cooling by fresh air). This allowed for the investigation of the thermal influence alone and the evaluation of the thermo-mechanical properties of the as-welded case.

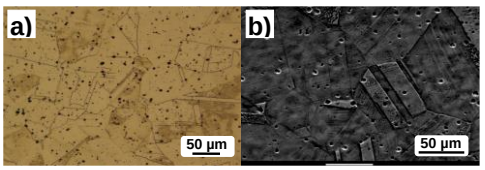

Fig. 1 Microstructure observation for AISI 316; a) by optical microscopic, b) by SEM.

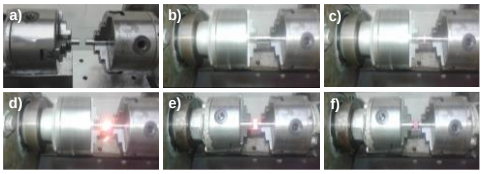

Fig. 2 Phases of friction welding process; a) holding of welding pieces, b, c and d) friction phase, e and f) forge phase.

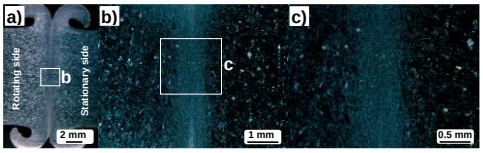

Fig. 3 Macroscopic observation shows grain refinement for welded joint centre.

RESULTS AND DISCUSSION

In DDFW, the two pieces are held tightly to the stationary and rotating chuck (**Fig. 2a**) and brought into contact with each other under the two most important factors: rotation speed and friction pressure. At this step, as shown in **Fig. 2b**, the temperature is very low, and the friction is too weak because rotation and pressure are responsible for that temperature elevation [21]. After a certain time does not exceed 3.5 s, the temperature increases quickly, and heat creation starts. The temperature at the interface is still limited between the two surfaces and leads to plasticizing the neighboring surfaces, as demonstrated in **Fig. 2c**. During the remaining period of friction, the accumulated heat in that part starts to diffuse and create the soft metal at the interface. Maintaining pressure applied leads to the transfer of soft metal from the interface toward the periphery to create flash, which continues to displace until the termination period of friction time (**Fig. 2d**). The speed of rotation ceases abruptly, and a high level of axial pressure is applied during the forge time to consolidate the weld (**Figs. 2e & f**). That forge is applied under the influence of forge temperature, which finally affects the nature of the welded joint [4].

Macroscopic observation obviously explains the amount of flash formation on both sides of the welded joint, as illustrated in **Fig. 3a**. The amount of flash is affected by DDFW conditions, such as rotation friction, friction pressure, friction time, and forge. Flash tends to increase with an increasing rotation speed [16], friction pressure [4], and friction time [13]. Forge, on the other hand, has a certain amount of influence on flash [20], and the position of the piece in the rotating or stationary side can affect the flash due to plastic deformation being higher on the stationary side than the rotating side [22].

Although mechanical [23] and physical [16] properties of weld metal, such as hardness, alloying elements [24], and thermoplastic deformation [25], also affect the flash. Present stainless steel is refractory due to containing high amounts of Cr, Ni, and Mo, and it requires more pressure and temperature to obtain the flash [3]. **Figs. 3b & c** reveal different magnifications for the narrow dimension of the welded joint center and show that there are no macro cracks or defects. Additionally, a certain uniform structure can be found in the center joint.

Microstructure observation for optical microscopy (**Fig. 4a**) and by SEM (**Fig. 4b**) for the welded joint center illustrate that the central region does not exceed 600 μm with grain refinement about 10 μm. This refinement is roughly three times that of the grain size of AISI 316, as shown in **Figs. 4c & d**. This region is usually identified as the dynamic recrystallized zone (DRZ) or HPDZ. Liu and Nelson [26] have clarified that dynamic recrystallization is frequently achieved for the material at hard plastic deformation and high temperature, and the welded joint interface will be carried out with heavily recrystallized grains. The initial grain size, metal chemical composition, deformation conditions, and crystal structure are the most significant factors affecting dynamic recrystallization. Titouche et al. [12] have mentioned that the temperature reached in the welding center and the mechanical stress attentiveness performed the recrystallization conditions that produced a fine grain. Azizieh et al. [16] have also revealed that the microstructure in the central region of the welded joint consists of fine grains microstructure resulting from high temperature and plastic deformation through friction welding process leading to dynamic recrystallization.

In the same opinion, the mechanical effect of dynamic recrystallization resulting from high forge pressure and elevated temperature could be responsible for defects in that region, such as microcavities (**Fig. 4d**). Previous studies [3, 21] considered the elimination and application of the forging phase have shown that the DRZ or HPDZ is created after forge pressure application under the influence of heat input and rotation cessation, resulting in a structure with fine grains and a fairly blackish color.

Additionally, AISI 316 austenitic stainless steel improves the microstructure, and grain refinement occurs in the welded joint due to hard plastic deformation resulting from the dynamic recrystallization of gamma iron grains [24]. Generally, this phenomenon occurs under the influence of high plastic deformation and elevated temperature, leading to the formation of welded joints with densely recrystallized grain forms [22].

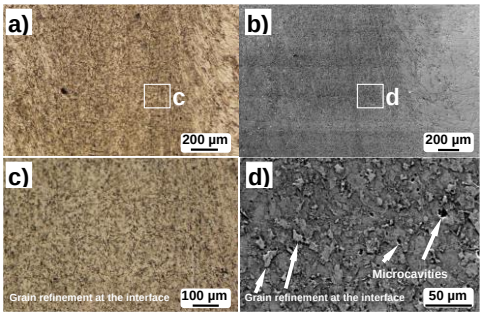

Fig. 4 Microscopic observation for welded joint with different magnification shows grain refinement; a and c) by optical microscopic, b and d) by SEM.

Figs. 5a & b demonstrate the investigation of the microstructure by optical microscopy and SEM, respectively, for the TMAZ adjacent to the welding interface. Partially deformed grains with larger and bent elongated forms are clearly observed as a result of the elevated heat input under the influence of high rotation speed (3000 rpm), friction pressure (130 MPa), and forge pressure (260 MPa) during the welding process. The TMAZ has grain growth with a size of about 100 μm, which is roughly three times larger than the grain size of AISI 316 and ten times related to HPDZ. Khidhir and Baban [24] explained that the TMAZ results from the speed of cooling at high temperature, which leads to grain growth.

Deformation twinning (**Fig. 6)** improves the microstructure and enhances mechanical properties by refining coarse grain structures during strain rate deformation processing, through subdivision of the grains and facilitating grain reorientation. Since smaller grains inhibit twinning, deformation twinning ceases below a critical grain size [27]. The microstructure characterization showed that the stir zone has an ultra-refined grain structure

with abundant twin boundaries by decreasing processing temperature. The main mechanisms of the grain refinement process were geometric dynamic recrystallization and twinning-induced dynamic recrystallization [28]. It is noteworthy that an increase in the number of twin directions is related to hardness [29], and the rotation of grains, particularly grains on both sides of a twin boundary, is responsible for twin decay [30].

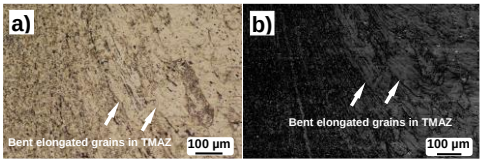

Fig. 5 Grain growth for adjacent regions (TMAZ); a) by optical microscopic, b) by SEM.

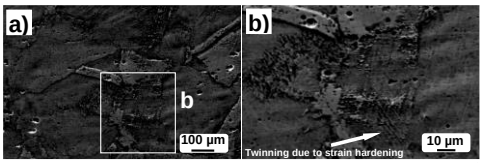

Fig. 6 Twins creation due to strain hardening at neighboring of the interface.

Fig. 7 shows the microhardness measurements achieved in the axial direction within 3 mm on the rotating side and 4.5 mm on the stationary side of the welded joint. The microhardness profile reveals an increase at the interface and a decrease in the neighboring region due to the creation of HPDZ and TMAZ, respectively. It also shows that there is no symmetric distribution between softening and hardening on the stationary and rotating sides, as there is a low mechanical action on the stationary side compared to the rotating side [25]. Two main aspects have to be considered to determine the values of microhardness: forge application and the interactive effect between friction and forge [31]. On the other hand, the increase in microhardness at the welding line can be explained by high plastic deformation and heating diffusion [32].

In general, grain refinement amplifies microhardness when the friction contact between surfaces at the interface during the FW process under axial pressure induces large plastic deformation guiding grain refinement. This creates the original foundation of the microhardness elevation at the welding center [12]. Conversely, Cr-Ni-Mo steel has a high amount of Mo which is responsible for the attenuation of microhardness in the neighboring region, leading the stainless steel to be extra refractory and reduce the speed of cooling rate and slow diffusion of heat, which causes the attenuation of microhardness [4].

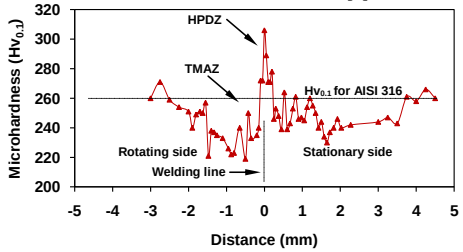

Fig. 7 Profile of microhardness by HV0.1 shows different values of microhardness in the welding center (HPDZ) and neighboring (TMAZ).

XRD analysis was performed for the welded joint and heat treated AISI 316 as well as for the base metal, heat treated processed at 819 °C with a soaking time of 30 min and cooling by fresh air, which led to determining thermal consequence alone and evaluating the thermo-mechanical effect of the welded joint. Fig. 8 reveals austenite reorganization and attentiveness at the level of 111 for heat treated and as-welded cases. At the same time, XRD confirms fine grain refinement in the welded joint, which is also evident in the microstructure of the welded joint, whereas in the heat treated case, there are moderately fine grains compared to AISI 316. The results of the XRD analysis were associated with microstructure and microhardness investigation in HPDZ creation and the increasing of microhardness at the welded joint, respectively.

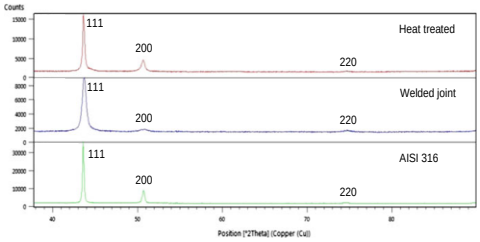

Fig. 8 XRD for welded joint and heat treated case related to AISI 316

CONCLUSIONS

Metallurgical investigation of AISI 316 using DDFW showed a narrow welding center with dimensions not exceeding 600 µm. Also, there were no macro cracks or defects, and a uniform joint center was discovered. The microstructure found HPDZ with grain refinement of approximately 10 µm, which is refining about three times compared to the grain size of AISI 316, and TMAZ was established adjacent with grain growth relatively 100 µm, which grows about three times related to AISI 316 and ten times related to HPDZ. On the other hand, a high level of microhardness at the welding center and a low level of microhardness at the neighboring region due to the formation of HPDZ and TMAZ, respectively. XRD demonstrated gamma iron concentration at the 111 levels due to grain refinement for the as-welded case due to high plastic deformation.

REFERENCES

1. D. Malhotra, A. S. Shahi: Metallurgical and Materials Transactions A, 51, 2020, 1647-1664. https://doi.org/10.1007/s11661-019-05623-0.
2. A. J. Hassan, T. Boukharouba, D. Miroud: Archives of Metallurgy and Materials, 67(3), 2022, 987-992. https://doi.org/10.24425/amm.2022.139692.
3. A. J. Hassan, T. Boukharouba, D. Miroud: International Journal of Advanced Manufacturing Technology, 112(7-8), 2021, 2223-2231. https://doi.org/10.1007/s00170-020-06421-4.
4. A. J. Hassan, T. Boukharouba, D. Miroud, N. Titouche, S. Ramtani: International Journal of Engineering Transactions C: Aspects, 33(12), 2514-2520, 2020, https://doi.org/10.5829/ije.2020.33.12c.12.
5. B. Vinith, S. A. D. Dharshan, S. Aravind, B. K. Singh: International Journal on Interactive Design and Manufacturing, 2023. https://doi.org/10.1007/s12008-023-01208-9.
6. V. Sinka: Acta Metallurgica Slovaca, 20(3), 2014, 287-294. https://doi.org/10.12776/ams.v20i3.312.

7. Y. Helal, Z. Boumerzoug: Acta Metallurgica Slovaca, 24(2), 2018, 163-173. https://doi.org/10.12776/ams.v24i2.1049.
8. E. Bouarroudj, S. Chikh, S. Abdi, D. Miroud: Applied Thermal Engineering, 110, 2017, 543-1553. https://doi.org/10.1016/j.applthermaleng.2016.09.067.
9. Y. Liu, H. Zhao, Y. Peng, X. Ma: Welding in the World, 64, 2020, 1799-1809. https://doi.org/10.1007/s40194-020-00960-w.
10. G. Wang, J. Li, J. Xiong, W. Zhou, F. Zhang: Welding in the World, 62, 2018, 1187-1193. https://doi.org/10.1007/s40194-018-0613-7.
11. H. Liu, H. Fujii: Materials Science & Engineering A, 800, 2021, 140303, https://doi.org/10.1016/j.msea.2020.140303.
12. N. Titouche, T. Boukharouba, S. Amzert, A. J. Hassan, R. Lechelah, S. Ramtani: Journal of Manufacturing Processes, 4, 2019, 273-283. https://doi.org/10.1016/j.jmapro.2019.03.016.
13. B. Cheniti, D. Miroud, R. Badji, P. Hvizdoš, M. Fides, T. Csanádi, B. Belkessa, M. Tata: Materials Science and Engineering A, 758, 2019, 36-46, https://doi.org/10.1016/j.msea.2019.04.081.
14. Y. Belkahla, A. Mazouzi, S. E l. Lebouachera, A. J. Hassan, M. Fides, P. Hvizdoš, B. Cheniti, D. Miroud: International Journal of Advanced Manufacturing Technology, 116, 2021, 2285–2298. https://doi.org/10.1007/s00170-021-07597-z.
15. A. J. Hassan, T. Boukharouba, D. Miroud: China Welding, 28(1), 2019, 42-48. https://doi.org/10.12073/j.cw.20180811001.
16. M. Azizieh, M. Khamisi, D. J. Lee, E. Y. Yoon & H. S. Kim: International Journal of Advanced Manufacturing Technology, 85, 2016, 2773-2781. https://doi.org/10.1007/s00170-015-8107-x.
17. H. Liu, Y. Aoki, Y. Aoki, K. Ushioda, H. Fujii: Journal of Materials Science and Technology, 46, 2020, 211-224, https://doi.org/10.1016/j.jmst.2019.10.037.
18. P. M. Ajith, T. M. A. Husain, P. Sathiya, S. Aravindan: Journal of Iron and Steel Research International, 22(10), 2015, 954-960. https://doi.org/10.1016/S1006-706X(15)30096-0.
19. M. Kimura, H. Sakaguchi, M. Kusaka, K. Kaizu, T. Takahashi: International Journal of Advanced Manufacturing Technology, 86, 2016, 2603-2614. https://doi.org/10.1007/s00170-016-8348-3.
20. M. Hazra, K. S. Rao, G. M. Reddy: Journal of Materials Research and Technology, 3(1), 2014, 90-100. https://doi.org/10.1016/j.jmrt.2013.12.001.
21. A. J. Hassan, T. Boukharouba, D. Miroud, N. E. Titouche, S. Ramtani: China Welding, 29(4): 2020, 7-12. https://doi.org/10.12073/j.cw.20200310001.
22. A. J. Hassan, T. Boukharouba, D. Miroud: Acta Metallurgica Slovaca, 26(3), 2020, 78–84. https://doi.org/10.36547/ams.26.3.631.
23. I. Kirik, N. Ozdemir: International Journal of Materials Research, 104(8), 2013, 769-775. https://doi.org/10.3139/146.110917.
24. G. I. Khidhir, S. A. Baban: Journal of Materials Research and Technology, 8(2), 2019, 1926-1932. https://doi.org/10.1016/j.jmrt.2019.01.010.
25. A. J. Hassan, T. Boukharouba, D. Miroud, S. Ramtani: International Journal of Engineering Transactions B: Applications, 32 (2), 2019, 306-312. https://doi.org/10.5829/ije.2019.32.02b.16.
26. F. C. Liu, T.W. Nelson: Material Characterization, 140, 2018, 39-44. https://doi.org/10.1016/j.matchar.2018.03.035.
27. S. Liu, D. Kent, N. Doan, M. Dargusch, G. Wang: Bioactive Materials, 4, 2019, 8-16. https://doi.org/10.1016/j.bioactmat.2018.11.001
28. N. Xu, Q. Song, Y. Bao, Y. Jiang, J. Shen, X. Cao. Science and Technology of Welding and Joining, 22(7), 2017, 610-616. https://doi.org/10.1080/13621718.2017.1286444.
29. S. Singh, N. R. Krishnaswamy, A. Soundraraj: Journal of Applied Physics, 27, 1956, 617-620. https://doi.org/10.1063/1.1722442.
30. S. Mishra, K. Narasimhan, I. Samajdar: Materials Science and Technology, 23(9), 2007, 1118-1126. https://doi.org/10.1179/174328407X213242.
31. V.V. Satyanarayana, R. G. Madhusudhan, T. Mohandas, Journal of Material Processing Technology, 160, 2005, 128-137. https://doi.org/10.1016/j.jmatprotec.2004.05.017.
32. I. Mitelea, V. Budau, C. Craciunescu: Journal of Material Processing Technology, 212, 2012, 1892-1899. https://doi.org/10.1016/j.jmatprotec.2012.04.010.